

# Bl Cuk Derived Pfc Converter for On-Board Ev Charger with Alternate Dc Source

KRISHNAPRIYA T NAIR<sup>1</sup>, RAHUL P RAJ<sup>2</sup>

<sup>1</sup>M-Tech, Power Electronics and Power System, Kerala Technical University

<sup>2</sup>Head of Department, Electrical and Electronics, KITS

**Abstract**— This article proposes a single-phase bridgeless Cuk-derived power factor corrected (PFC) converter with a smaller number of components is proposed for on-board EV charging applications. The distinctive feature of this proposal is to design and operate the output inductance of the converter in discontinuous current mode for the whole power range to achieve the PFC naturally on the AC grid, which eliminates the need to sense the input voltage and current. This reduces the cost of the converter and improves the power density as well as the robustness of the converter against high frequency disturbances. Thanks to a sophisticated circuit design and the optimization of the components, the converter achieves a considerable reduction in the total number of components and thus contributes to cost efficiency and a compact design. The control of the converter is very simple in operation and easy to implement with only a single sensor-based voltage control loop. The voltage stress of the semiconductor components of the proposed converter is lower compared to the traditional converter. It also contains an alternative direct current source from a fuel cell. This research represents a significant leap forward in the field of EV charging technology. The reduced number of components increases reliability, lowers costs and contributes to the development of more sustainable and efficient electric transportation.

**Index Terms**— Bridgeless converter, efficiency, electric vehicle (EV), on-board charging, optimization of components, power factor correction (PFC), sustainable transport.

## I. INTRODUCTION

Battery-powered electric vehicles contribute to a cleaner and quieter ecosystem while reducing operating and transportation costs. These technologies fall within the sphere of interest of the government and car manufacturers and are therefore supported by various government development programs. In 2019, there were 5.6 million electric cars on the road, but current market research suggests that there will be

more than 1 billion electric cars on the road by 2040 and 2050. These EVs are powered by high-voltage 400 V batteries. Therefore, a battery charger is required to charge the EV's power source. There are currently two types of battery chargers available on the market:

- 1) on-board chargers and
- 2) off-board chargers

The chargers essentially convert the variable AC input voltage into the required DC voltage and current. An on-board charger requires a power factor corrected (PFC) converter at the front end of the power supply to meet the harmonic limits set by the standards. A typical battery charger consists of an AC filter at the input, followed by an AC to DC boost PFC converter with DC bus capacitors connecting the isolated DC to DC converter to the PFC converter. Finally, a DC output filter is connected at the end. Numerous topologies are proposed for charging electric vehicles on board. The two-stage configurations consist of an active PFC converter in the first stage, followed by an isolated DC/DC converter. The two-stage topologies have the advantage of being easy to implement. However, the main disadvantages are the higher number of components, the high costs and the relatively low efficiency due to the processing of the total power in two conversion stages. Therefore, the single-stage configurations are reported. The single-stage structures usually consist of an uncontrolled diode bridge rectifier and a DC/DC converter. The high conduction loss of the diode bridge rectifier at the input requires a different solution, namely the elimination of the diode bridge rectifier, which is known as bridgeless (BL) topologies. Although the reported BL topologies solve the diode bridge problem, they still have the same number of components as the conventional ones. Therefore, in this article, a novel BL Cuk-derived bridge-less PFC converter for on-board EV chargers with alternative

DC source and fewer number of components with a simple control scheme was proposed.

## II. COMPARISON BETWEEN EXISTING SYSTEM AND PROPOSED SYSTEM

- a. Instead of two stage topologies with higher number of components, the proposed system having only single stage structure with reduced number of components.
- b. Reduces cost, increases power density as well as converter robustness to high frequency noise.
- c. The existing system need input current and voltage sensing for PFC correction, but the proposed system is simple to operate, easy to implement and effective in achieving PFC with simple control and simple sensor only.

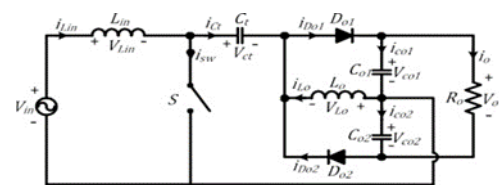
## III. OBJECTIVES

- a. This project aims to propose a single phase bridgeless Cuk- derived PFC converter with fewer number of components for on board EV charging application.
- b. The unique feature of this proposal is the DCM operation of the output inductor for complete converter power range to attain PFC naturally at ac mains without the need of traditional input voltage and input current sensors.
- c. It can also be works on an alternate DC source from a fuel cell.

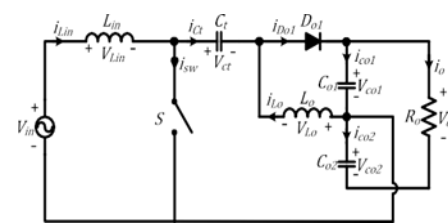
## IV. PROPOSED SYSTEM

The proposed single-phase BL CUK converter is shown in Fig. 1(a). The total number of components required to implement the proposed power converter is eight. It consists of a bidirectional switch, two output diodes, two inductors and a total of three capacitors. This is two less than the traditional Cuk converter, which requires 10 components to implement the converter. The two power switches are connected back-to-back to ensure the bidirectional blocking function and are controlled by a common gate signal, i.e. they are turned on and off simultaneously. The configuration of the proposed power circuit during positive and negative half cycles is shown in Fig. 1(b) and (c) respectively. During the

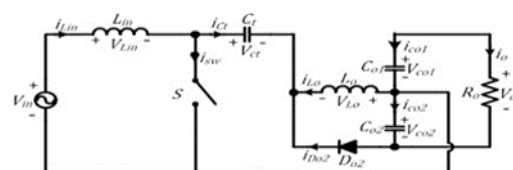
positive half cycle, the output diode “Do1” is active, while the output diode “Do2” is active during the negative half cycle. It is worth noting that either the switch or only one diode is in the current path during the entire operation of the converter. This reduces conduction losses and simplifies the thermal management of the power converter. Another key feature of the proposed power converter is the lower voltage stress ( $V_m + \frac{V_o}{2}$ ) of the semiconductor devices compared to the conventional voltage stress ( $V_m + V_o$ ) of the Cuk converter, which reduces switching losses and increases the operating efficiency of the converter. The inductance at the output of the power converter is designed to operate in discontinuous current conduction mode over the entire power range of the power converter in order to achieve a natural PFC on the AC input side. The voltage at the output of the power converter is controlled by a simple voltage control loop as shown in Fig. 1(d). Based on this simple loop, the power converter operates at a constant duty cycle for a given output voltage and output power, as the duty cycle depends only on the error between the reference and measured voltage. As a result, the power converter requires only one voltage sensor at the output, which reduces the cost of the battery charger and increases its robustness and reliability.



(a)



(b)



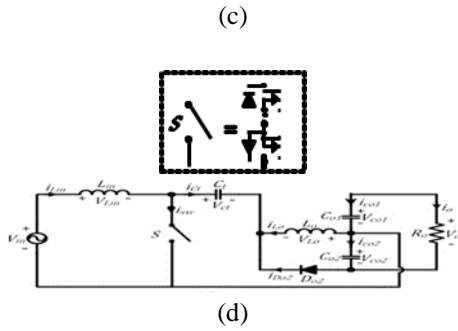


Fig. 1(a) Proposed single-phase bridgeless Cuk-based converter. (b), (c) Converter configurations during positive and negative half-cycles. (d) Output voltage control circuit for proposed converter.

### V. WORKING OF THE SYSTEM

The operation of the proposed converter during positive and negative half cycles are similar. So, the power converter analysis is discussed for positive half cycle only. Fig. 2 depicts a complete switching cycle with discontinuous output inductor current waveform of the proposed converter during positive half cycle. In the proposed BL CUK derived converter, the current discontinuity in the output diode defines the discontinuous current mode. Three modes of operation are observed in a single switching cycle for the proposed converter. The operation of the converter is described as follows:

Mode-1 (to - t1): The "S" switch "is active in this mode and the output diodes are inactive. Before entering this mode, the current at input " $i_{Lin}$ " freewheels in the loop formed by " $V_{in}$ ", " $L_{in}$ ", " $C_t$ " and " $L_o$ " and is displayed as " $i_{fw}$ ". The inductance at the input " $L_{in}$ " stores the energy of the supply source " $V_{in}$ " and the inductance at the output " $L_o$ " stores the energy of the transfer capacitor " $C_t$ " with a gradient of " $V_{in}/L_{in}$ " or " $V_{in}/L_o$ ".

$$i_{Lin} = i_{fw} + \frac{V_{in}}{L_{in}}t \quad (1)$$

$$i_{Lo} = -i_{fw} + \frac{V_{in}}{L_o}t \quad (2)$$

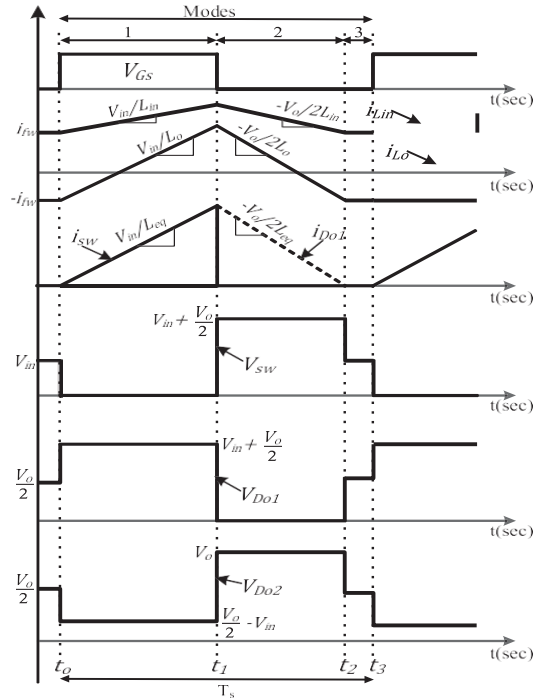


Fig. 2. Proposed converter waveform during positive half cycle.

Mode-2 (t1 - t2): Switch "S" is inactive in this mode and the diode at output " $D_{o1}$ " is active. Prior to enter this mode, the inductance at the input and the inductance at the output have reached their maximum values. If the "S" switch "is inactive, the entire switch current is taken over by the diode at the " $D_{o1}$ ," output. The inductance at the input and the inductance at the output are demagnetized by transferring the stored energy to the output load, while the capacitor at the output " $C_{o1}$ ," and the transfer capacitor " $C_t$ " are charged:

$$c = i_{fw} + \frac{V_{in}}{L_{in}}DT_s - \frac{V_o}{2L_{in}}t \quad (3)$$

$$i_{Lo} = -i_{fw} + \frac{V_{in}}{L_o}DT_s - \frac{V_o}{2L_o}t \quad (4)$$

where  $DT_s$  is equal to a  $t_{on}$  represents the active period of the switch. The mode ceases when the current passing through diode " $D_{o1}$ " drops to zero, indicating

$$i_{Lin} + i_{Lo} = 0 \quad (5)$$

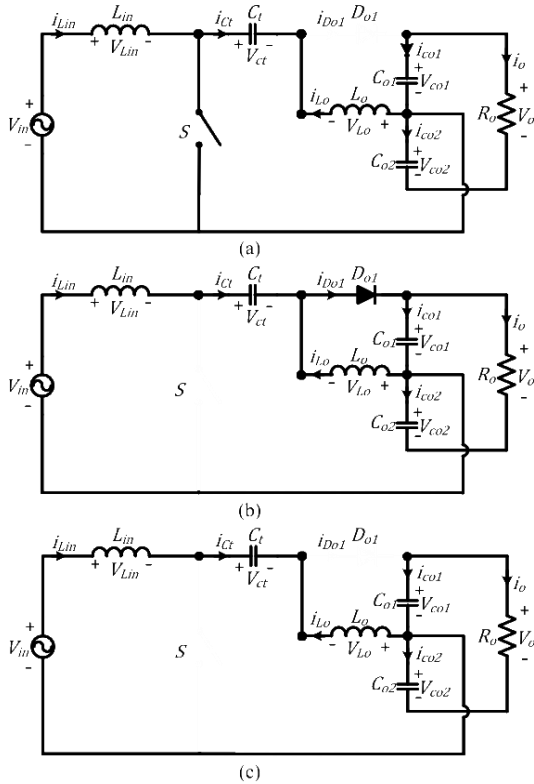


Fig. 3. Converter equivalent circuits. (a) Mode-1, (b) Mode-2, (c) Mode-3.

By solving equation (5), we obtain

$$D1T_s = \frac{2V_{in}}{V_o} DT_s \tag{6}$$

$D1T_s$  signifies the second mode time period.

Mode-3 ( $t_2 - t_3$ ): The illustrated equivalent circuit of the power converter applies to this specific mode. All semiconductor devices are not active, while the load is supplied by the output capacitors.

**A. Condition of Operation Involving Discontinuous Current Flow**

The discontinuous current operation of the power converter has been verified, when

$$DT_s + D1T_s \leq T_s \tag{7}$$

$$D \leq \frac{M}{M + 2\sin\omega t} \tag{8}$$

Where  $V_{in} = V_m \sin\omega t$  and  $M = \frac{V_o}{V_m}$ .

From the above equation, the minimum duty cycle occurs when  $\sin\omega t = 1$ , which implies  $\omega t = \frac{\pi}{2}$ .

Therefore, the requirement for power converter discontinuous current operation is:

$$D \leq \frac{M}{M + 2} \tag{9}$$

The critical value for voltage conversion ratio for a specific duty cycle can be determined from equation (9), is expressed as;

$$M_{cr} \geq \frac{2D}{1 - D} \tag{10}$$

$M_{cr}$  is the parameter that determines the critical voltage conversion ratio. In order for the power converter to function properly, it is necessary for the voltage at the output to exceed two times the maximum input voltage to reverse bias the diodes. Consequently, the power converter must have a voltage gain sufficient for this requirement to be met.

$$M \geq M_{cr} \geq 2 \tag{11}$$

**B. Average Output Current**

The average current at the output of the power converter during a complete switching cycle is equal to the average current of diode "D<sub>01</sub>" at the output. Because of the triangular form of the current flowing through the output diode, its average value can be determined by using

$$i_{D01,avg} = \frac{i_{D01,pk} D_1 T_s}{2T_s} \tag{12}$$

Where,  $i_{D01,avg} = \frac{V_{in}}{L_{eq}} DT_s$  is the maximum value of diode at output "D<sub>01</sub>" current, and  $L_{eq} = \frac{L_{in} L_o}{L_{in} + L_o}$ .

Solving equation (12),

$$i_{D01,avg} = \frac{V_m^2 D^2 T_s}{L_{eq} V_o} \sin^2 \omega t \tag{13}$$

The power converter average output current for a line period is obtained by integrating equation (13) for a half period;

$$i_{D01,avg} = \frac{V_m^2 D^2 T_s}{4L_{eq} V_o} \tag{14}$$

**C. Passive Components Design**

Peak current ripple of input inductor " $\Delta i_{Lin}$ " is given by

$$\Delta i_{Lin} = \frac{V_m}{L_{in}} DT_s \tag{15}$$

$$L_{in} = \frac{V_m}{\Delta i_{Lin}} DT_s \tag{16}$$

The inductor at the output " $L_o$ " is given as

$$L_o = \frac{L_{in} L_{eq}}{L_{in} - L_{eq}} \tag{17}$$

The value of  $L_{eq}$  is obtained from (9) and (14),

$$L_{eq} \leq \frac{V_m^2 V_o^2 T_s}{4P_o (v_o + 2V_m)^2} \tag{18}$$

Where  $P_o$  is nominal load power.

Assume  $C_{o1} = C_{o2} = C_o$ , the low frequency voltage ripple at output can be determined by

$$\Delta V_{o,ripple} = \frac{1}{C_o} (\int i_{Co1} dt + \int i_{Co2} dt) \quad (19)$$

$$\Delta V_{o,ripple} = \frac{1}{C_o} (\int i_{Do1,avg} - 2i_o) dt = \frac{2i_o}{\omega C_o} \quad (20)$$

$$C_o = \frac{2i_o}{\omega \Delta V_{o,ripple}} \quad (21)$$

The design of the transfer capacitor " $C_t$ " is of crucial importance, as it has a major influence on the quality of the input current and the value should be determined in such a way that no low-frequency oscillations occur with the inductances at the output and input. therefore, the resonant frequency " $f_r$ " caused by the intermediate capacitor " $C_t$ " must have a value that lies between the switching frequency and the mains frequency:

$$f_{in} \ll f_r \ll f_s \quad (22)$$

Where  $f_{in}$  = input supply frequency,  $f_s$  = switching frequency, and  $f_r = \frac{1}{2\pi\sqrt{C_t(L_{in}+L_o)}}$ .

The converter in Fig. 1(a) was modeled and simulated in PSIM 11. The input specifications and the design results are shown in Tables 1 and 2 respectively.

TABLE I  
INPUT SPECIFICATIONS

Parameter	Value
Input Voltage ( $V_{in}(rms)$ )	120 V
Output Voltage ( $V_o$ )	400 V
Output Power ( $P_o$ )	1kW
Output Voltage Ripple ( $V_{o,ripple}$ )	2%
Input Current Ripple ( $I_{in,ripple}$ )	8%
Switching Frequency ( $f_{sw}$ )	50kHz
Line Frequency ( $f_{line}$ )	60Hz

TABLE II  
DESIGN PARAMETERS

Parameter	Value
Maximum Duty Cycle ( $D_{max}$ )	0.541
Input Inductor ( $L_{in}$ )	1.5mH
Output Inductor ( $L_o$ )	29μH
Transfer Capacitor ( $C_t$ )	2.3μF
Output Capacitor ( $C_{o1}, C_{o2}$ )	1.66mF

TABLE III  
COMPONENTS SPECIFICATION

Components	Specifications
------------	----------------

MOSFET	UJ3CO65030K3S, Sic 650 V, 35mΩ
Diodes	60EPF12, 1200 V, 60 A
Input Inductor ( $L_{in}$ )	159ZL-C14H, 1.8 mH, at 50 kHz
Output Inductor ( $L_o$ )	E 55/28/21 Ferrite core, 29μH
Transfer Capacitors ( $C_t$ )	R71P134704030M, 0.47μF * 5
Output Capacitors ( $C_{o1}, C_{o2}$ )	ESMQ401VSN471MQ50W, 470μF * 3
DSP	TMS320F28335
Gate Driver	IC-IXYS-IXDN609SI
Power Source	California Instruments ASTI503
Voltage sensor	LV25-P

## VI. SIMULATION AND EXPERIMENTAL RESULTS

Fig 4(a) shows simulation diagram of the proposed system. Because the plant switch characteristic is a single-pole machine, a proportional integral (PI) controller ( $K_i/s + K_p$ ) is deployed sufficient for the acquisition of essential machine response. With a bandwidth of less than 754 rad/s and a section margin (PM) of 60°, the controller tuning is completed using the MATLAB Siso tool. 60% damping and 10% overrun translate into a 60° PM. The received switch characteristic is listed in (28). It is possible to calculate the costs of  $k_i$  (= 0.28286) and  $k_p$  (= 0.0062). The machine's ability to maintain a steady-state voltage without making errors may be comprehended by looking at its open-loop switch characteristic, which offers an infinite benefit at lower frequencies. Additionally, the resilience of the load change disturbance and source voltage are established. Utilizing the LV25-P Hall-effect sensor, the output voltage is sensed. By programming the TI-DSP-TMS320F28335 to generate PWM signals for the gate of the power converter's MOSFETs, the designed controller is implemented in real-time. This is accomplished primarily by comparing the sensed

voltage to a reference voltage, and the resulting error is provided as an input to the PI controller, which outputs the duty cycle and serves as the input for the saturation block. A 50 kHz sawtooth waveform is used to compare the saturation block's output. Consequently, the power MOSFETs generate their PWM signals. A limiter is positioned to prevent the power converter from entering CCM and to safeguard against overload:

$$G(s) = \frac{V_0(s)}{D(s)} = \frac{1030}{0.1333s+1} \quad (23)$$

$$H(s) = \frac{0.28286}{s} + 0.006 \quad (24)$$

$$G(s) * H(s) = \frac{1030*(0.28286+0.0062s)}{s(0.133s+1)} \quad (25)$$

The output voltage and current from the AC supply source, the fuel cell's output voltage and current, the simulation results for the capacitors, and the converter's unity power factor operating at full load are all displayed below.

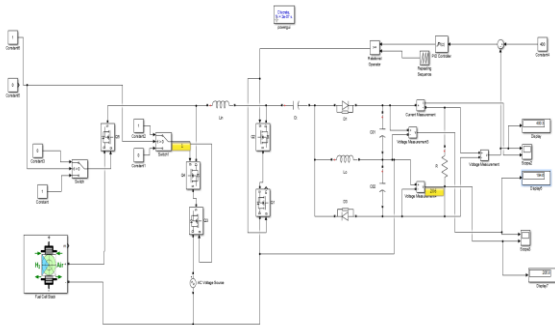


Fig. 4(a). Simulation diagram

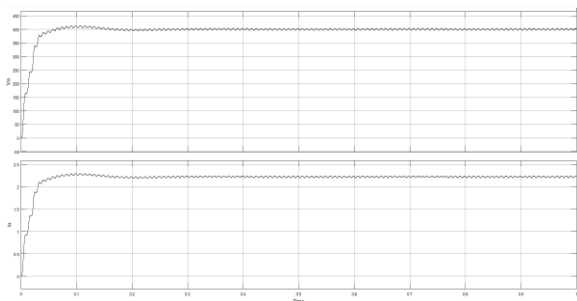


Fig. 4(b). Output voltage and output current from AC supply

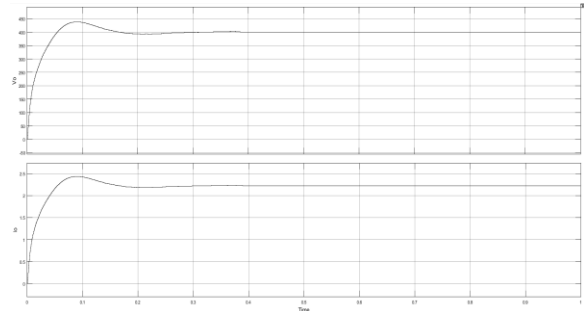


Fig. 4(c). Output voltage and output current from DC source

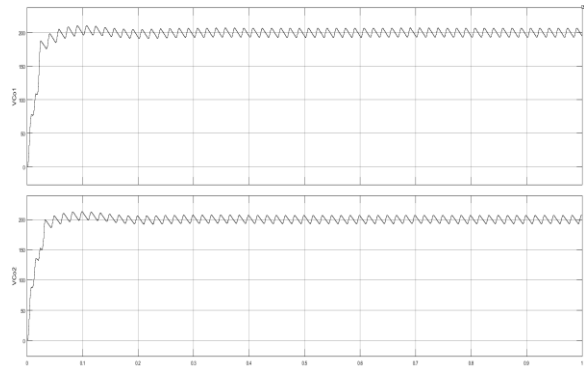


Fig. 4(d). Output capacitor and output voltage

Fig. 4(b) shows the output voltage and output current response at rated output power from an AC supply source, while Fig. 4(c) shows the response from an alternate DC source. Fig. 4(d) displays the voltages across output capacitors with a constant output voltage of 400 V and a voltage ripple of 8 V (2% as intended), in line with the analysis. Table III displays the parts utilized in the experimental configuration. The input inductor is created with the worst-case voltage situation in mind and a maximum input current ripple of 8%.

## CONCLUSION

This article presents and examines a novel BL single-phase Cuk-derived PFC converter with a reduced number of components for use as an on-board charger. The power converter's inductor at the output is intended to operate in discontinuous current conduction mode throughout the power range to achieve natural PFC at the AC input side. This reduces the need for sensors, cutting operation costs, increasing the converter's resilience to high-frequency noise, and providing high density. The new single-

phase Cuk-based power converter reduces component voltage stress compared to the traditional Cuk PFC converter, leading to lower switching losses and increased overall efficiency of the power converter. Furthermore, only one semiconductor device is conducting current in the entire converter operation range. Therefore, reducing power converter losses from conduction, and facilitating thermal management. The primary advantages include the simplicity of topology, the effectiveness of the control, and the practicality of the solution. This article provides a concise overview of multiple BL Cuk-derived circuit configurations. Analysis of the power converter in steady-state conditions using a single switching. The process of cycling is thoroughly explained, including the development of design equations and transfer functions.

#### REFERENCES

- [1] C. C. Chan and K. T. Chau, "An overview of power electronics in electric vehicles," *IEEE Trans. Ind. Electron.*, vol. 44, no. 1, pp. 3–13, Feb. 1997, doi: 10.1109/41.557493.
- [2] A. Dixit, K. Pande, S. Gangavarapu, and A. K. Rathore, "DCM- based bridgeless PFC converter for EV charging application," *IEEE J. Emerg. Sel. Topics Ind. Electron.*, vol. 1, no. 1, pp. 57–66, Jul. 2020, doi: 10.1109/JESTIE.2020.2999595.
- [3] "Limits for harmonic current emissions (Equipment input current <16A per phase)," IEC/EN61000-3-2, 1995.
- [4] J. G. Pinto, V. Monteiro, H. Gonçalves, and J. L. Afonso, "Onboard reconfigurable battery charger for electric vehicles with traction-to-auxiliary mode," *IEEE Trans. Veh. Technol.*, vol. 63, no. 3, pp. 1104–1116, Mar. 2014, doi: 10.1109/TVT.2013.2283531.
- [5] K. Yoo, K. Kim, and J. Lee, "Single- and three-phase PHEV onboard battery charger using small link capacitor," *IEEE Trans. Ind. Electron.*, vol. 60, no. 8, pp. 3136–3144, Aug. 2013.
- [6] "Asia-Pacific electric three-wheeler market (2013–2023)," Research And- Markets.com, para. 1, Oct. 2018. [Online]. Available: <https://www.researchandmarkets.com/research/14k8s8/asiapa>
- [7] R. Kushwaha and B. Singh, "Interleaved landsman converter fed EV battery charger with power factor correction," in *Proc. IEEE 8th Power India Int. Conf.*, 2018, pp. 1–6.
- [8] A. Y. Saber and G. K. Venayagamoorthy, "Plug-in vehicles and re- newable energy sources for cost and emission reductions," *IEEE Trans. Ind. Electron.*, vol. 58, no. 4, pp. 1229–1238, Apr. 2011, doi: 10.1109/TIE.2010.2047828.
- [9] H. V. Nguyen and D. Lee, "Advanced single-phase onboard chargers with small DC-link capacitors," in *Proc. IEEE Int. Power Electron. Appl. Conf. Expo.*, 2018, pp. 1–6.
- [10] A. Emadi, M. Ehsani, and J. M. Miller, *Vehicular Electric Powersystems: Land, Sea, Air, and Space Vehicles*. New York, NY, USA: Marcel Dekker, 2003.
- [11] S. Gangavarapu, A. K. Rathore, S. K. Mishra, and R. K. Singh, "Analysis and design of a single-phase bridgeless Cuk-based PFC converter as on-board charger with reduced number of components and losses," in *Proc. IEEE Transp. Electrific. Conf.*, 2019, pp. 1–6, doi: 10.1109/ITEC-India48457.2019.ITECINDIA2019-194.
- [12] Y. Lee, A. Khaligh, and A. Emadi, "Advanced integrated bidirectional AC/DC and DC/DC converter for plug-in hybrid electric vehicles," *IEEE Trans. Veh. Technol.*, vol. 58, no. 8, pp. 3970–3980, Oct. 2009, doi: 10.1109/TVT.2009.2028070.
- [13] A. Hajimiragha, C. A. Canizares, M. W. Fowler, and A. Elkamel, "Optimal transition to plug-in hybrid electric vehicles in Ontario, Canada, consid- ering the electricity-grid limitations," *IEEE Trans. Ind. Electron.*, vol. 57, no. 2, pp. 690–701, Feb. 2010, doi: 10.1109/TIE.2009.2025711
- [14] H. Li, S. Wang, Z. Zhang, J. Tang, X. Ren, and Q. Chen, "A SiC bidi- rectional LLC on-board charger ," in *Proc. IEEE Appl. Power Electron. Conf. Expo.*, 2019, pp. 3353–3360.
- [15] D. Patil, M. Sinha, and V. Agarwal, "A Cuk converter based bridgeless topology for high power factor fast battery charger for electric vehi- cle application," in *Proc. IEEE Transp.*

*Electric. Conf. Expo.*, 2012, pp. 1–6.

- [16] H. J. Chae, W. Y. Kim, S. Y. Yun, Y. S. Jeong, J. Y. Lee, and H. T. Moon, “3.3kW on board charger for electric vehicle,” in *Proc. 8th Int. Conf. Power Electron. Asia*, 2011, pp. 2717–2719.
- [17] R. Kushwaha and B. Singh, “An improved battery charger for electric vehicle with high power factor,” in *Proc. IEEE Ind. Appl. Soc. Annu. Meeting*, 2018, pp. 1–8.
- [18] A. A. Fardoun, E. H. Ismail, A. J. Sabzali, and M. A. Al-Saffar, “New efficient bridgeless Cuk rectifiers for PFC applications,” *IEEE Trans. Power Electron.*, vol. 27, no. 7, pp. 3292–3301, Jul. 2012.